



Article

A Multi-GNSS/IMU Data Fusion Algorithm Based on the Mixed Norms for Land Vehicle Applications

Chen Jiang ¹, Dongbao Zhao ¹, Qiuzhao Zhang ^{2,*}  and Wenkai Liu ¹

¹ College of Surveying and Geo-Informatics, North China University of Water Resources and Electric Power, Zhengzhou 450046, China; jiangchen@ncwu.edu.cn (C.J.)

² School of Environment Science and Spatial Information, China University of Mining and Technology, Xuzhou 221116, China

* Correspondence: qiuzhao.zhang@cumt.edu.cn; Tel.: +86-(0371)69127696

Abstract: As a typical application of geodesy, the GNSS/INS (Global Navigation Satellite System and Inertial Navigation System) integrated navigation technique was developed and has been applied for decades. For the integrated systems with multiple sensors, data fusion is one of the key problems. As a well-known data fusion algorithm, the Kalman filter can provide optimal estimates with known parameters of the models and noises. In the literature, however, the data fusion algorithm of the GNSS/INS integrated navigation and positioning systems is performed under a certain norm, and performance of the conventional filtering algorithms are improved only under this fixed and limited frame. The mixed norm-based data fusion algorithm is rarely discussed. In this paper, a mixed norm-based data fusion algorithm is proposed, and the hypothesis test statistics are constructed and adopted based on the chi-square distribution. Using the land vehicle data collected through the multi-GNSS and the IMU (Inertial Measurement Unit), the proposed algorithm is tested and compared with the conventional filtering algorithms. Results show that the influences of the outlying measurements and the uncertain noises are weakened with the proposed data fusion algorithm, and the precision of the estimates is further improved. Meanwhile, the proposed algorithm provides an open issue for geodetic applications with mixed norms.

Keywords: chi-square; covariance inflation; data fusion; multi-GNSS/IMU; mixed norms



Citation: Jiang, C.; Zhao, D.; Zhang, Q.; Liu, W. A Multi-GNSS/IMU Data Fusion Algorithm Based on the Mixed Norms for Land Vehicle Applications. *Remote Sens.* **2023**, *15*, 2439. <https://doi.org/10.3390/rs15092439>

Academic Editors: Serdjo Kos, Juan F. Prieto and José Fernández

Received: 12 April 2023

Revised: 28 April 2023

Accepted: 1 May 2023

Published: 6 May 2023



Copyright: © 2023 by the authors. Licensee MDPI, Basel, Switzerland. This article is an open access article distributed under the terms and conditions of the Creative Commons Attribution (CC BY) license (<https://creativecommons.org/licenses/by/4.0/>).

1. Introduction

It is well known that GNSS is able to provide precise information of the position and velocity under a favorable observation environment, and the positioning errors do not accumulate over time. Thus, the GNSS technique has been applied in broad fields for many years [1–3]. Although different satellite navigation and positioning systems can be selected and the number of visible satellites is increasing, the performance of GNSS can be degraded by the signal problems, such as the lock-lost and unknown interferences. On the other hand, no signal is sent and received by INS, and it has been widely applied in the navigation of kinematic carriers. INS can provide precise and short-term navigation and positioning information, and the observation frequency is much higher than that of the GNSS receivers. Moreover, INS has many other advantages such as anti-electronic jamming. Nevertheless, the positioning errors of INS accumulate quickly over time [4], especially for the low-cost IMU, hence it cannot independently undertake the task of long-term navigation under fast kinematic conditions. Naturally, the properties of GNSS and INS are complementary, and the integrated systems provide an ideal solution in kinematic positioning and navigation applications [5–7].

One of the most imperative techniques for the GNSS/INS integrated navigation systems lies in the data fusion, and the most frequently used data fusion recursive algorithm for the discrete linear system is the Kalman filter [8,9]. In the Kalman filter, the estimates

are optimal when the models and statistical information of the noises are exactly known. However, in the practical applications of the Kalman filter, the prior models and statistical information of the noises can hardly be specified due to the complex environment and uncertain circumstances. Thus, some outlying measurements and uncertain errors may significantly degrade the performance of the filtering. Moreover, the conventional Kalman filter is applicable for linear systems only, but more systems in practice exert nonlinear characters [10]. Aimed at addressing the shortcomings of the conventional Kalman filter, many types of filters were developed in practical applications. These improved filters mainly consist of nonlinear filters, robust filters and adaptive filters, et al. The extended Kalman filter (EKF) was proposed to deal with the nonlinear problem, and it is one of the most commonly used nonlinear Kalman filters. Proximate with the EKF, other types of nonlinear filters were proposed based on different norms, such as the particle filter [11], the unscented Kalman filter (UKF) [12] and the cubature Kalman filter (CKF) [13,14], et al. The central difference is that the Kalman filter (CDKF) can also conduct the nonlinear transformation by polynomial fitting [15]. With these nonlinear filters, the applications of the Kalman filter are extended further. The outlier detection method was developed to control the influences of the outlying measurements with a relatively low efficiency [16]. Then, the detection, identification and adaptation, namely, the D.I.A. methods were developed [17], but the process of identification is still a difficult problem. Based on the robust estimation theory and other robust algorithms, the robust filter was developed to weaken the influences of the outliers by the covariance inflation factor [18].

In terms of the model errors and the uncertain noises, a series of adaptive filters were developed. For the adaptive filters, the function model-based and the stochastic model-based adaptive filters are conventional solutions. Then, the multiple model-based and the innovation-based adaptive estimation were developed and applied in the GNSS/INS integrated navigation systems [19]. Furthermore, Chinese researchers developed a different type of adaptive filter through the adaptive factor [20], and four different factors and detection statistics were constructed and applied in the kinematic navigation and positioning field. Similarly, the finite impulse response filter was developed against the model errors. This filter requires no noise statistics and is not so sensitive to the model errors [21]. The centroid weighted Kalman filter is another improved filter aimed at the state model and the observation model uncertainty, and the centroid weighted method is applied to optimize the predicted state value [22]. By minimizing the estimated error in the worst case, the H_∞ filter was proposed to control the uncertain noises in the measurements. However, the performance may be seriously degraded under an abnormal environment [23], and may be improved if the outliers are controlled effectively. By integrating the advantages of different state estimation filters, their combination becomes another way to improve the filtering performance. For example, the applications of the particle filter are limited by the problem of particle degradation, and this problem can be improved with the suitable and precise importance density function [24,25]. In order to solve this problem, the Kalman filter, the EKF, the UKF, and the CKF are adopted to construct the importance density function. Thus, the Kalman particle filter, the extended particle filter, and the unscented particle filter were proposed and applied [26,27]. Based on the reduced INS and the GNSS, an autonomous vehicle sideslip angle estimation algorithm was proposed based on the consensus and the vehicle kinematics/dynamics synthesis, and a multi-sensor framework was developed [28,29]. This framework provides an important and extendable platform for multi-sensor integration; for example, the IMU and automotive onboard sensors are integrated to estimate the yaw misalignment [30]. Under the above framework, the vehicle dynamics/kinematics fusion algorithm was proposed and applied in the actual experiments [31]. There are, of course, other filtering algorithms not discussed in this paper.

For the GNSS/INS integrated navigation systems, the current data fusion algorithm is performed under a certain norm, and most improved algorithms were also developed under this fixed frame. Therefore, performance of the conventional filtering algorithms are improved and compared under this fixed frame as well. Under this background, in

order to test and compare the performance out of the fixed frame, another algorithm should be explored and developed. In literature, the multiple norm-based algorithm is rarely discussed. In fact, different norms correspond to different performance of the filtering, and mixed norm-based algorithms can combine the advantages of different algorithms. In the fields of mathematics and computer techniques, the mixed norm-correlated algorithm was discussed and applied in face recognition, et al., and the validity of the constructed algorithm was demonstrated [32]. Accordingly, the mixed norm-based algorithm may become a new and quite different way to improve the solution of the GNSS/INS integrated navigation systems, and the algorithm with mixed norms may achieve a better performance compared with the conventional filtering algorithm.

In this paper, a new data fusion algorithm is proposed and applied in the actual data processing work of the multi-GNSS/IMU integrated systems. Contrary to the conventional data fusion algorithms, the proposed data fusion algorithm for the multi-GNSS/IMU integrated systems is implemented based on the mixed norms, and this improvement is performed from the perspective of the application of different cost functions. In the proposed algorithm, the measurements for the data fusion are addressed with the hypothesis test, and the hypothesis test statistics are constructed based on the chi-square to distinguish different circumstances. The application of different circumstances depends on the results of the hypothesis test, and the different norm is adopted to estimate the state parameters under different circumstances. Besides different cost functions, the covariance inflation factor is duly applied according to the results of the hypothesis test to weaken the influences of the outlying measurements.

The rest of this paper is listed as follows. First, the corresponding theory of the Kalman filter and the H_∞ filter is introduced, and the nonlinear H_∞ filter is applied. Second, the basic equations of the GNSS/INS integrated navigation systems are provided and discussed. Third, different experiments are designed and performed with the actual data to test the performance of the proposed filtering scheme. Last, the conclusions are summarized.

2. Kalman Filter and H_∞ Filter

In the kinematic positioning and navigation fields, the Kalman filter is the basic data fusion algorithm. Meanwhile, the Kalman filter provides the basic structure of the filter, and many improved filters are developed based on the Kalman filter.

2.1. Iterative Solution of the Kalman Filter

Assume that x_k is the parameter vector, $\Phi_{k,k-1}$ is the transition matrix of x_k , x_{k-1} is the estimated state vector at the epoch $k-1$, w_k is the system noise, z_k is the observation vector, H_k is the observation matrix, and v_k is the observation noise. Then the kinematic model and the observation model are defined by:

$$\begin{cases} x_k = \Phi_{k,k-1}x_{k-1} + w_k \\ z_k = H_kx_k + v_k \end{cases} \quad (1)$$

In the conventional Kalman filter, the processes of time update and measurement update are listed below [8]:

$$x_{k,k-1} = \Phi_{k,k-1}x_{k-1} \quad (2)$$

$$P_{k,k-1} = \Phi_{k,k-1}P_{k-1}\Phi_{k,k-1}^T + Q_k \quad (3)$$

$$x_{k,k} = x_{k,k-1} + K_k(z_k - H_kx_{k,k-1}) \quad (4)$$

$$K_k = P_{k,k-1}H_k^T(H_kP_{k,k-1}H_k^T + R_k)^{-1} \quad (5)$$

$$P_k = P_{k,k-1} - K_kH_kP_{k,k-1} \quad (6)$$

where $x_{k,k-1}$ is the predicted state vector at the epoch k , $P_{k,k-1}$ is the covariance matrix of $x_{k,k-1}$, P_{k-1} is the covariance matrix of x_{k-1} , Q_k is the covariance matrix of w_k , $x_{k,k}$ is the estimated state vector at the epoch k , K_k is the gain matrix, R_k is the covariance matrix of v_k , and P_k is the covariance matrix of x_{k-1} . In the conventional Kalman filter, it should be noted that the extremum condition is defined as follows:

$$V_k^T R_k^{-1} V_k + V_{x_{k,k-1}}^T P_{k,k-1}^{-1} V_{x_{k,k-1}} = \min \tag{7}$$

where V_k and $V_{x_{k,k-1}}$ are the residuals of z_k and $x_{k,k-1}$, respectively.

2.2. Principles of the H∞ Filter

With the given restricted parameter γ , the H∞ filter was proposed to overcome the uncertain interference in the measurements [18]. Simultaneously, assume that y_k is another state vector, and $y_k = L_k x_k$, where L_k is usually a fixed matrix. Contrary to the conventional Kalman filter, the exact statistical information of the noises need not be known. For the cost function J :

$$J = \frac{\sum_{k=1}^N \|x_k - \hat{x}_k\|^2}{\|x_0 - \hat{x}_0\|_{P_0}^2 + \sum_{k=1}^N (\|w_k\|_{Q_k}^2 + \|v_k\|_{R_k}^2)} \tag{8}$$

where \hat{x}_0 and \hat{x}_k are the estimated state vectors of x_0 and x_k , respectively, x_0 is the initial value of the state vector x , and P_0 is the covariance matrix of x_0 . With this cost function, the parameters are estimated when $\hat{x}_k = \operatorname{argmin} \|J\|_\infty$. Performance of the filter is determined by the threshold parameter γ , and improper value of γ may cause a negative definite covariance or filter divergence. It should be noted that the H∞ filter can be robust to some extent through changing the value of γ , but it breaks down in the face of outliers [18]. Therefore, the threshold parameter γ should be fixed appropriately according to the detailed applications and performance.

In practice, more systems are nonlinear, and the linear H∞ filter should be transformed to the nonlinear filter. In order to implement the nonlinear transformation, assume that $P_{k,k-1} H_k^T = P_{xz,k}$ and $H_k P_{k,k-1} H_k^T = P_{zz,k} - R_k$, and $P_{xz,k}$ and $P_{zz,k}$ are the innovation covariance matrix and the cross-covariance matrix, respectively. Then, the covariance matrix of the state vector in the nonlinear H∞ filter is given by:

$$P_{k,k} = P_{k,k-1} - [P_{xz,k} P_{k,k-1}] \begin{bmatrix} P_{zz,k} - R_k + I & P_{xz,k}^T \\ P_{xz,k} & P_{k,k-1} - \gamma^2 I \end{bmatrix}^{-1} \begin{bmatrix} P_{xz,k}^T \\ P_{k,k-1}^T \end{bmatrix} \tag{9}$$

Through the above transformation, the linear can be implemented in the nonlinear filters.

Apparently, both the conventional Kalman filter and the H∞ filter are performed under a single and certain norm, and this becomes the main difference between the conventional filters and the proposed filtering algorithm of this paper.

3. Proposed Data Fusion Algorithm Based on the Mixed Norms

3.1. Multi-GNSS/IMU Integration and the Chi-Square-Based Hypothesis Test

In the kinematic positioning and navigation field, a single navigation technique can hardly be suitable for all scenarios. Therefore, the integrated navigation technique becomes the ideal choice for different scenarios. The combination of GNSS and INS is one of the commonly used integrated navigation techniques, and it has been adopted in broad applications. With the Multi-GNSS and the IMU, the loosely-coupled integration mode is applied in this paper, and the CKF is applied to deal with the nonlinear problem. Errors of the position, velocity, and attitude of the kinematic carrier, and the bias of the accelerometer and the gyroscope are the parameters of the state vector \hat{x} , namely,

$$\hat{x} = [\Delta R^e \ \Delta V^e \ \varphi^e \ \varepsilon^b \ \nabla^b] \tag{10}$$

where e and b denotes the variates defined under the earth frame and the body frame, respectively. With the cubature Kalman filter, the iterative solution of the state parameters is derived as follows:

$$x_{k,k} = x_{k,k-1} + K_k(z_k - H_k x_{k,k-1}) \quad (11)$$

$$K_k = P_{xz,k,k-1} P_{zz,k,k-1}^{-1} \quad (12)$$

$$P_{k,k} = P_{k,k-1} - K_k P_{zz,k,k-1} K_k^T \quad (13)$$

where the measurement vector z_k consists of the position and velocity differences between GNSS and IMU.

For the kinematic model and the observation model in Equation (1), the models are usually known and exact when the measurements meet the Gaussian distribution. Assume that \bar{z}_k ($\bar{z}_k = H_k x_{k,k-1}$) and $P_{\bar{z}_k}$ are the mean and the covariance of the measurements, respectively, then the probability density function $\rho(z_k)$ of z_k is given by:

$$\rho(z_k) = N(z_k; H_k x_{k,k-1}, P_{\bar{z}_k}) = \frac{\exp\left(-\frac{1}{2}(z_k - H_k x_{k,k-1})^T (P_{\bar{z}_k})^{-1} (z_k - H_k x_{k,k-1})\right)}{\sqrt{(2\pi)^m |P_{\bar{z}_k}|}} \quad (14)$$

where m is the dimension of z_k , and $|P_{\bar{z}_k}|$ is the determinant of $P_{\bar{z}_k}$. If no outliers exist, $\rho(z_k)$ is suitable to depict the measurements. Otherwise, another probability density function should be constructed. Therefore, whether the initial probability density function holds or not can be treated as the condition to detect the outlying measurements. Considering the probability density function, the expression $(z_k - H_k x_{k,k-1})^T (P_{\bar{z}_k})^{-1} (z_k - H_k x_{k,k-1})$, namely, the square of the Mahalanobis distance from z_k to \bar{z}_k , is adopted as the error detection statistic [33]. Assuming $(z_k - H_k x_{k,k-1})^T (P_{\bar{z}_k})^{-1} (z_k - H_k x_{k,k-1})$ equals D_M^2 and the quantile of a fixed confidence level is marked as χ_α , D_M^2 should obey the chi-square distribution if the measurements are normal, and D_M^2 should be less than χ_α . Otherwise, some outliers may exist and their influences should be eliminated or weakened. Therefore, the chi-square hypothesis test based on the Mahalanobis distance is adopted to detect the abnormal observation environment.

In the face of the outliers, the common strategy is to eliminate the corresponding measurements or decrease the outlying measurements' weights. Therefore, the robust estimation method and the covariance inflation factor λ_{ij} are introduced. λ_{ij} is calculated based on the standardized predicted residual, and the covariance matrix of the measurements is redefined by:

$$\bar{R}_k = \lambda_{ij} R_k \quad (15)$$

Consequently, aimed at the uncertain noises and the outliers, a new multi-GNSS/IMU data fusion algorithm is proposed based on the mixed norms and the chi-square hypothesis test, and the effects of the outlying measurements are controlled through the covariance inflation factor. Then, the proposed algorithm is applied and compared with the conventional algorithms in the multi-GNSS/IMU integrated navigation systems.

3.2. Theoretical Analysis of the Proposed Algorithm

On one hand, the hypothesis test process of the proposed data fusion algorithm is similar with that of the conventional fault detection method, and they are both implemented at each epoch with the fixed confidence level. On the other hand, it is quite different in terms of the filtering calculation process. In the proposed algorithm, the filtering calculation process is implemented according to the result of the hypothesis test. The null hypothesis will be accepted if D_M^2 is less than χ_α , and the cubature Kalman filter should be performed based on the Equation (7). Otherwise, the null hypothesis should be rejected, and the nonlinear H_∞ filter will be performed. For the static positioning, the position information

4. Experiments and Analysis

The performance of the proposed data fusion algorithm is applied and tested in the data processing of the multi-GNSS/IMU integrated navigation systems. The main equipment of the multi-GNSS/IMU integrated navigation systems consist of two GNSS receivers and an IMU, and the IMU consists of the three-axis accelerometers and the three-axis fiber-optic gyroscope. The GNSS receivers are Trimble R8 geodetic receivers, and they were set to receive the signals of multiple GNSS constellations. One of the receivers was set as the reference station, and another receiver, together with the IMU, was set on the land vehicle to detect its position, velocity, and attitude information. The equipment of these integrated systems is plotted in Figure 2. The nominal RMSE (Root Mean Square Error) for the GNSS receivers and the key technical specifications of the IMU are provided in Table 1.



Figure 2. The basic equipment of the integrated systems.

Table 1. Key technical specifications of the GNSS receivers and the IMU.

Sensor	Bias	Scale Factor	Random Walk	RMSE	Sample Interval
Accelerometer	50 mgal	4000 ppm	55 $\mu\text{g}/\text{rt-Hz}$ (velocity random walk)	—	0.01 s
Gyroscope	20 deg/h (rate bias)	1500 ppm	0.067 deg/h ^{1/2} (angle random walk)	—	
GNSS receiver	—	—	—	Position: 0.5 m; Velocity: 0.05 m/s	1 s

The experiment dataset was collected with the above multi-GNSS/IMU integrated navigation systems. The diagonal elements of the covariance matrix correspond to the errors of the position, and the velocity was set as 0.25 m² and 0.0025 m²/s², respectively. According to the technical specifications, the initial position and velocity bias are set to 1.0 m and 0.1 m/s, respectively. After mechanization, the observation information of the IMU and GNSS is constructed and input into the filter. According to the dataset, the motion trajectory and distance of the land vehicle is plotted in Figure 3.

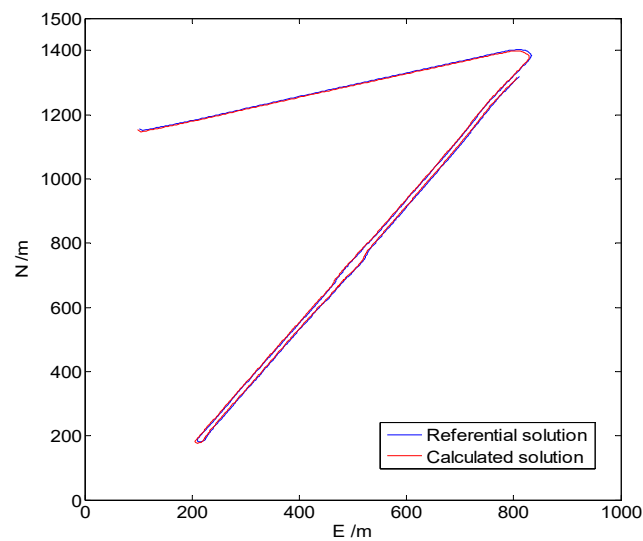


Figure 3. Motion trajectory and distance of the land vehicle in north and east directions. The trajectory shows that the land vehicle moves in an almost straight direction, except for several turns. The red line denotes the referential solution, and the blue line denotes the solution calculated with self-developed software.

In the experiments, two different cases were designed and organized to compare the performance of different algorithms. Each case consisted of four different algorithms, and these four algorithms were implemented with the same dataset, respectively. The GNSS double-difference carrier phase results calculated from the commercial Inertial Explorer software were adopted as the referential solution, and the results of all four algorithms were compared with the referential solution, respectively. These four algorithms are listed below.

Algorithm 1: the cubature Kalman filter (CKF);

Algorithm 2: the H_∞ filter based on the cubature Kalman filter (HF);

Algorithm 3: the mixed norm-based filter with the confidence level of 95% (MC-95);

Algorithm 4: the mixed norm-based filter with the confidence level of 99% (MC-99);

For the H_∞ filter of the above algorithms in each case, the threshold parameter γ was set to 2.

4.1. Case 1

In this case, the four designed algorithms were performed with the initial dataset, respectively. In the filtering process of this paper, the predicted state vector consist of fifteen elements, and the first three elements are the position error variables during the filtering. The values of these three elements of the predicted state vector for different algorithms are plotted in Figures 4–7.

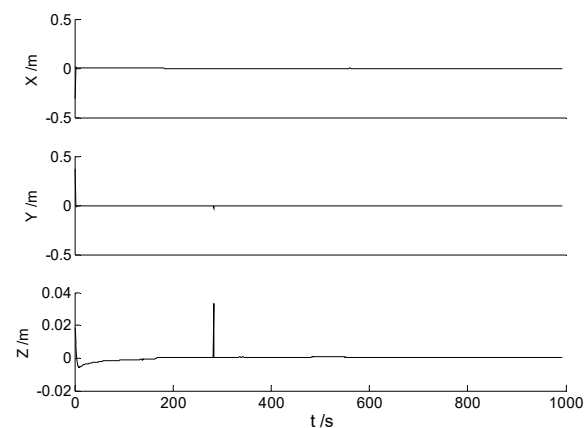


Figure 4. The position error variables of the predicted state vector for the CKF.

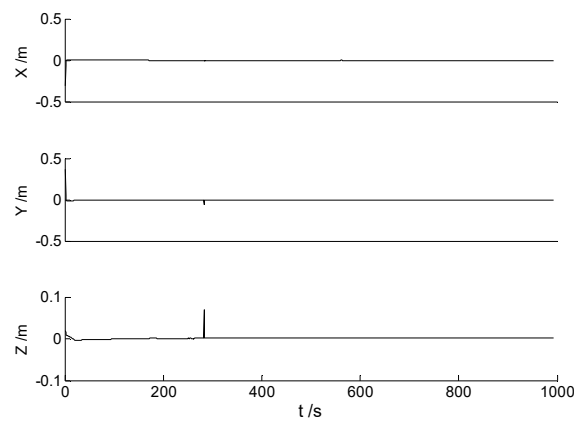


Figure 5. The position error variables of the predicted state vector for the HF.

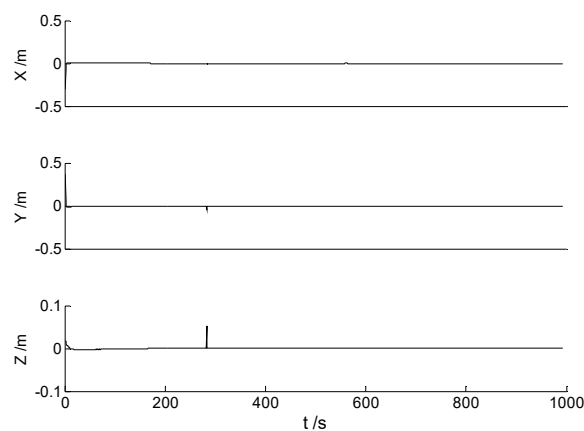


Figure 6. The position error variables of the predicted state vector for the MC-95.

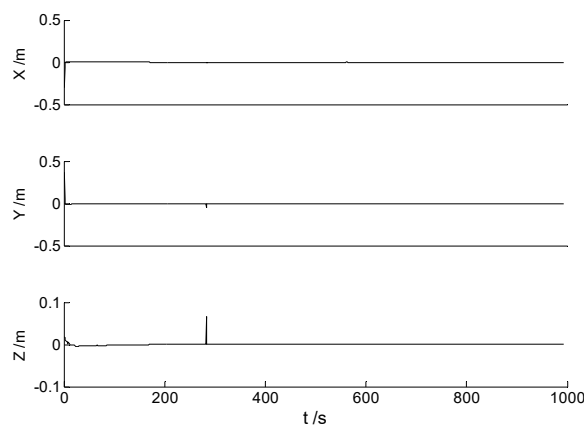


Figure 7. The position error variables of the predicted state vector for the MC-99.

Figures 4–7 demonstrate the position error variables of the predicted state vector for different algorithms. It is found from the above figures that the values of these variables are quite small. However, these are just the process variables, and can hardly demonstrate the performance of different algorithms. Since the final position errors (namely, the differences between the referential solution and the calculated solution) are easier to demonstrate the differences of these algorithms, they are plotted to distinguish the performance of different algorithms. Then, the differences from the referential solution of different algorithms are demonstrated in Figures 8–11.

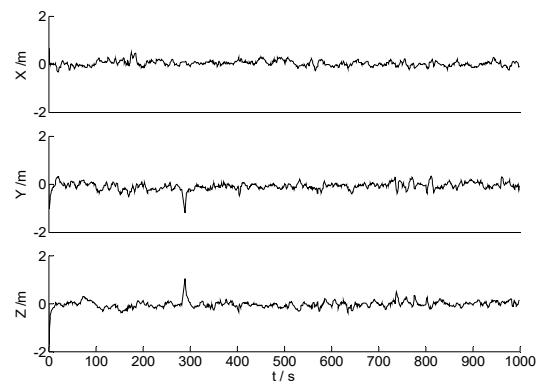


Figure 8. Position errors of the CKF.

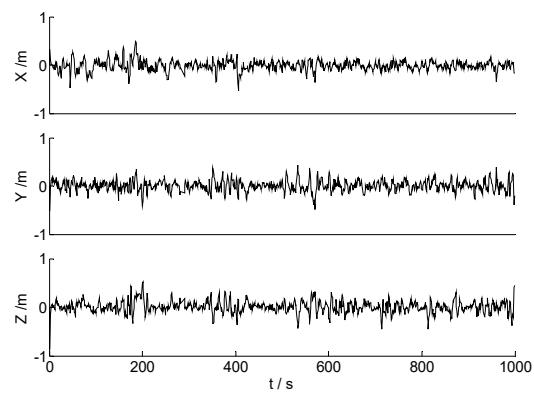


Figure 9. Position errors of the HF.

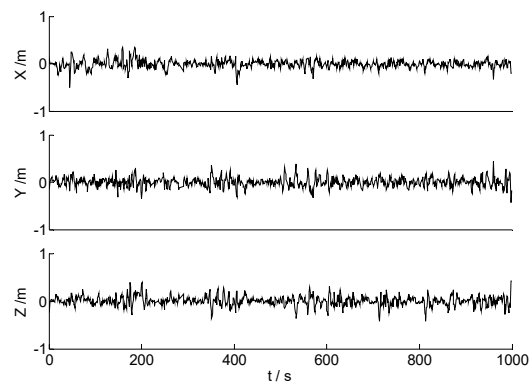


Figure 10. Position errors of the MC-95.

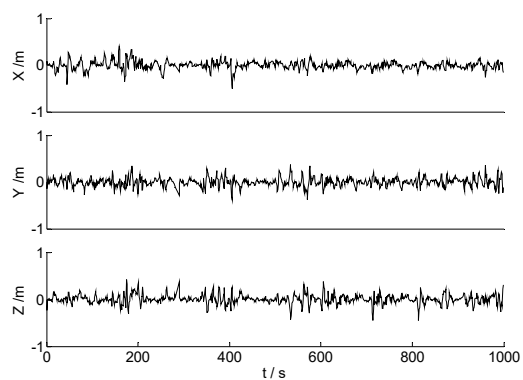


Figure 11. Position errors of the MC-99.

As the land vehicle travels on the urban road, the complex environment may bring some unpredictable influences to the signals, such as the shelter, the electromagnetic interference, and other uncertain noises. When the land vehicle travels over the speed bumps, the equipped sensors generate an abnormal vibration. This results in some apparent disturbances, as demonstrated in Figure 8. Therefore, the apparent disturbance indicates that the CKF algorithm is sensitive to the abnormal measurements, and the ability of robustness for the CKF algorithm should be enhanced further. Compared with the CKF algorithm, the performance of the HF algorithm plotted in Figure 9 manifests an apparent ability of robustness. Since the dataset contains little disturbances, the null hypothesis is accepted at most epochs, and performance of the algorithms 2–4 is mainly determined by the H_{∞} filter. Accordingly, in Figures 9–11, the positioning errors of different algorithms are similar, since the process of the H_{∞} filter is relatively stable. In practical applications, the position of the carrier, together with its velocity and attitude, are important parameters to help to make decisions. Therefore, the RMSE of the position (P_x , P_y , P_z), the velocity (V_x , V_y , V_z) and the attitude (Pitch, Yaw) for different algorithms are adopted to depict their performance quantitatively, and the statistical information is presented in Table 2.

Table 2. RMSE of different algorithms in Case 1.

Algorithm	P_x (m)	P_y (m)	P_z (m)	V_x (m/s)	V_y (m/s)	V_z (m/s)	Pitch (Degree)	Yaw (Degree)
CKF	0.12	0.17	0.15	0.10	0.12	0.13	1.05	2.13
HF	0.11	0.14	0.13	0.03	0.04	0.06	0.97	1.98
MC-95	0.09	0.09	0.11	0.03	0.03	0.06	0.80	0.86
MC-99	0.09	0.10	0.11	0.02	0.03	0.05	0.82	1.27

Table 2 demonstrates that the RMSE values of the CKF algorithm are bigger than those of the other algorithms, especially the RMSE values of the velocity and the attitude. This indicates that the performance of the CKF algorithm is improved by the H_{∞} filter, since the uncertain noises were well controlled. Compared with the HF algorithm, the MC-95 and MC-99 algorithms performed better with the relatively smaller RMSE values. In fact, for the MC-95 and MC-99 algorithms, the influences of the abnormal measurements were weakened, and the IMU measurements became more accurate after the closed-loop feedback. Compared with the MC-95 algorithm, the null hypothesis was rejected at more epochs in the MC-99 algorithm. More measurements were detected and identified as abnormal, and the weights of these measurements were degraded in the filtering. Therefore, the parameters estimated through the multi-GNSS/IMU integrated navigation systems are more likely to be precise and reliable.

4.2. Case 2

In this case, some significant outliers (40 m) were artificially added into the initial GNSS measurements; thus, the second dataset was constructed. Then, the four designed algorithms were implemented with the second dataset, respectively. Similarly, the position differences from the referential solution are demonstrated in Figures 12–15, respectively.

In Figures 12 and 13, it is demonstrated that both the CKF and the HF algorithms are seriously affected by the significant outliers. Compared with the CKF algorithm, the HF algorithm exerts stronger robustness, and the influences of the significant outliers are weakened further. For the algorithms with mixed norms, the amplitudes of the position errors become much smaller, and no apparent outlying value is found in Figures 14 and 15. This indicates that the effects of the outlying measurements are controlled effectively. In contrast to the MC-95 algorithm, the MC-99 algorithm performs the hypothesis test with a smaller quantile, and more outlying measurements are detected and identified. Therefore, the MC-99 algorithm performs better with the relatively smaller error amplitudes, and the filtering become more stable. It is worth noticing that the threshold should not be too small, as the data utilization efficiency is decreased with an unreasonably small threshold, and the

precision of the filtering may become inferior under this scenario. Therefore, the reasonable threshold should be set according to the practical applications. Then, the corresponding statistical information is provided in Table 3.

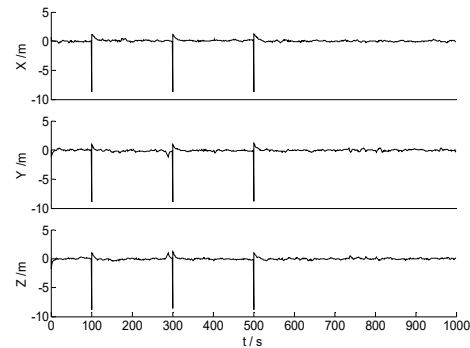


Figure 12. Position errors of the CKF.

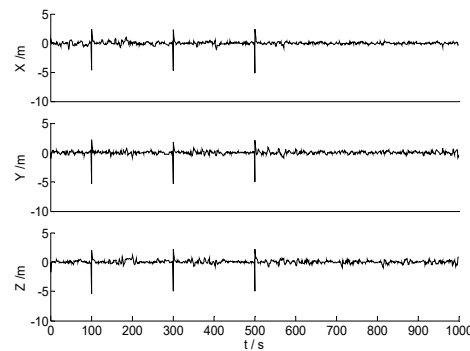


Figure 13. Position errors of the HF.

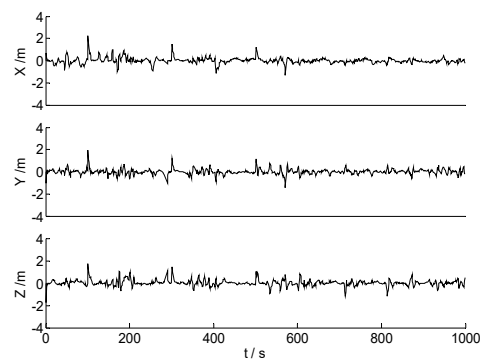


Figure 14. Position errors of the MC-95.

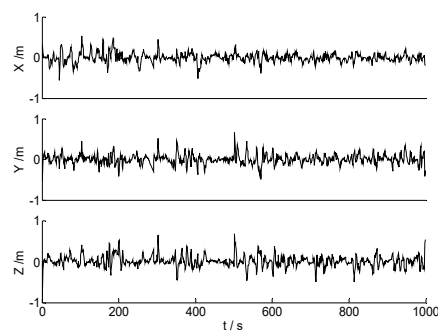


Figure 15. Position errors of the MC-99.

Table 3. RMSE of different algorithms in Case 2.

Algorithm	P_x (m)	P_Y (m)	P_z (m)	V_x (m/s)	V_Y (m/s)	V_z (m/s)	Pitch (Degree)	Yaw (Degree)
CKF	0.51	0.52	0.55	0.18	0.16	0.15	1.29	2.36
HF	0.37	0.39	0.47	0.05	0.07	0.08	1.01	2.05
MC-95	0.13	0.12	0.20	0.04	0.06	0.06	0.86	1.49
MC-99	0.11	0.10	0.12	0.04	0.05	0.05	0.84	1.34

In this case, the influences of the significant outlying measurements become the main factor that affects the precision of the estimates, and it is suitable to test the robustness of different algorithms. In Table 3, the RMSE values indicate that the precision of different algorithms are degraded by the significant outliers, and the RMSE values of the CKF and HF algorithms are several times bigger than those in Case 1, respectively. In terms of the errors of the position, the velocity and the attitude, influences to the velocity and the attitude of the significant outliers are lighter than those in the position. RMSE values of both the MC-95 and MC-99 algorithms are much smaller than those of the CKF and HF algorithms, since the advantages of the H_∞ filter and the robust estimation method are combined in the mixed norm-based filtering. Comparing the CKF and the mixed norm-based algorithms, it is demonstrated that the precision of the velocity and the attitude are improved with the mixed norm-based algorithms. For the MC-95 algorithm, considering Tables 2 and 3, it can be summarized that it is more likely to achieve a better attitude estimation precision with the mixed norm-based algorithms. In this case, the outlying measurement often has an affect not only at the current epoch, but also at the following several epochs. Namely, the significant outliers may cause some new outliers, and the influences at the following epochs usually become lighter than the initial significant outliers. In the hypothesis test, the smaller the threshold, the more outliers can be detected and identified, and the influences of the outliers can be weakened further with the smaller to some extent. Consequently, the MC-99 algorithm performed better than the MC-95 algorithm in this case. Moreover, along with the development of the intelligent PNT (Positioning, Navigation and Timing), more sensors and other available information are integrated and applied in the vehicle positioning, such as the camera [35], the high definition map [36], the laser radar [37], et al. The integration of multiple sensors combines the advantages of different sensors, but the data fusion should always be addressed carefully. Meanwhile, as these above two cases have demonstrated, the proposed data fusion algorithm provides another way to improve the performance of the multi-sensor integration systems, and it can provide some useful references in the practical applications of the parameter estimation.

5. Conclusions

For the data fusion algorithm of the multi-GNSS/IMU integrated navigation systems, the conventional filtering algorithm and most improved algorithms are developed under a single certain norm. In this paper, a different way to improve the performance of the filtering is explored, and a new multi-GNSS/IMU data fusion algorithm with mixed norms is proposed. In the proposed algorithm, the hypothesis test statistics are constructed based on the chi-square distribution to distinguish different scenarios, and the filtering algorithm under different norms is implemented according to different scenarios. The detailed conclusions summarized from the experiments of this paper are listed below.

- (1) Compared with the conventional cubature Kalman filter, the H_∞ filter manifests a better ability of robustness, since the influences of the uncertain noises are controlled effectively, and the precision of the estimated parameters are improved. However, the performance of the cubature Kalman filter and the H_∞ filter is affected significantly by the outlying measurements.
- (2) Besides the filtering algorithms, collecting a valid and stable dataset is still an important way to achieve a better filtering solution. A relatively higher precision of

the velocity and the attitude estimated in the multi-GNSS/IMU integrated navigation systems is achieved with the H_∞ filter, regardless of the existence of some outlying measurements.

- (3) By integrating the advantages of the robust estimation and different filtering algorithms, a better performance is achieved with the mixed norm-based algorithms. In this paper, the results of these experiments indicate that it is more likely to achieve a better attitude estimation precision with the mixed norm-based algorithms, but a reasonable threshold for the hypothesis test should be set according to the detailed applications.
- (4) In this paper, the cubature Kalman filter and the H_∞ filter are selected to construct the mixed norm-based parameter estimation algorithms. Therefore, it is still an open issue to construct different algorithms with different norms, and can provide another way to improve the filtering performance in practical data processing applications.

Author Contributions: C.J. put forward the algorithm, designed the experiments methods, and prepared this manuscript; D.Z. and Q.Z. helped to discuss the experimental results; and W.L. reviewed the whole manuscript. All authors have read and agreed to submit the manuscript.

Funding: This research was partially supported by the Pre-research Project of Songshan Laboratory (YYJC062022013) and the Natural Science Foundation of Henan Province (212300410198).

Data Availability Statement: The data supporting the results in this paper can be obtained through the email jcdtdtg@163.com.

Conflicts of Interest: The authors declare no conflict of interest.

References

1. Yang, Y.X.; He, H.B.; Xu, T.H. Adaptive robust filtering for kinematic GPS positioning. *Acta Geod. Et Cartogr. Sin.* **2001**, *30*, 293–298.
2. Godha, S.; Cannon, M.E. GPS/MEMS INS integrated system for navigation in urban areas. *GPS Solut.* **2007**, *11*, 193–203. [[CrossRef](#)]
3. Yang, Y.; Xu, J. GNSS receiver autonomous integrity monitoring (RAIM) algorithm based on robust estimation. *Geod. Geodyn.* **2016**, *7*, 117–123. [[CrossRef](#)]
4. Cui, B.; Chen, X.; Tang, X. Improved cubature Kalman filter for GNSS/INS based on transformation of posterior sigma-points error. *IEEE Trans. Signal Process.* **2017**, *65*, 2975–2987. [[CrossRef](#)]
5. Jiang, W.; Liu, D.; Cai, B.; Rizos, C.; Wang, J.; Shangguan, W. A Fault-Tolerant Tightly Coupled GNSS/INS/OVS Integration Vehicle Navigation System Based on an FDP Algorithm. *IEEE Trans. Veh. Technol.* **2019**, *68*, 6365–6378. [[CrossRef](#)]
6. Chiang, K.; Tsai, G.; Chang, H.; Joly, C.; El-Sheimy, N. Seamless navigation and mapping using an INS/GNSS/grid-based SLAM semi-tightly coupled integration scheme. *Inf. Fusion* **2019**, *50*, 181–196. [[CrossRef](#)]
7. Doostdar, P.; Keighobadi, J.; Hamed, M.A. INS/GNSS integration using recurrent fuzzy wavelet neural networks. *GPS Solut.* **2020**, *24*, 1–15. [[CrossRef](#)]
8. Kalman, R.E. A new approach to linear filtering and prediction problems. *J. Basic Eng.* **1960**, *82*, 35–45. [[CrossRef](#)]
9. Zhong, M.Y.; Guo Yang, Z.H. On real time performance evaluation of the inertial sensors for INS/GPS integrated systems. *IEEE Sens. J.* **2016**, *16*, 6652–6661. [[CrossRef](#)]
10. Ma, C.; Pan, S.; Gao, W.; Ye, F.; Liu, L.; Wang, H. Improving GNSS/INS Tightly Coupled Positioning by Using BDS-3 Four-Frequency Observations in Urban Environments. *Remote Sens.* **2022**, *14*, 615. [[CrossRef](#)]
11. Majidi, M.; Erfanian, A.; Khaloozadeh, H. Prediction-discrepancy based on innovative particle filter for estimating UAV true position in the presence of the GPS spoofing attacks. *IET Radar Sonar Navig.* **2020**, *14*, 887–897. [[CrossRef](#)]
12. Impraimakis, M.; Smyth, A.W. An unscented Kalman filter method for real time input-parameter-state estimation. *Mech. Syst. Signal Process.* **2022**, *162*, 108026. [[CrossRef](#)]
13. Zhao, Y.W. Performance evaluation of cubature Kalman filter in a GPS/IMU tightly-coupled navigation system. *Signal Process.* **2016**, *119*, 67–79. [[CrossRef](#)]
14. Arasaratnam, I.; Haykin, S.; Hurd, T.R. Cubature Kalman filtering for continuous-discrete systems: Theory and simulations. *IEEE Trans. Signal Process.* **2010**, *58*, 4977–4993. [[CrossRef](#)]
15. Amini Tehrani, H.; Bakhshi, A.; Yang, T.Y. Online jointly estimation of hysteretic structures using the combination of central difference Kalman filter and Robbins–Monro technique. *J. Vib. Control.* **2021**, *27*, 234–247. [[CrossRef](#)]
16. Almas, M.A.; Sharma, K. A two stage mean and iterative median filter approach for image denoising. *Int. J. Adv. Sci. Technol.* **2020**, *29*, 5355–5361.

17. Teunissen, P.J.G. Quality control in integrated navigation systems. In Proceedings of the 1990'-A Decade of Excellence in the Navigation Sciences, IEEE PLANS'90 Position Location and Navigation Symposium, Las Vegas, NV, USA, 20 March 1990; pp. 158–165.
18. Chang, G. Robust Kalman filtering based on Mahalanobis distance as outlier judging criterion. *J. Geod.* **2014**, *88*, 391–401. [[CrossRef](#)]
19. Mohamed, A.H.; Schwarz, K.P. Adaptive Kalman filtering for INS/GPS. *J. Geod.* **1999**, *73*, 193–203. [[CrossRef](#)]
20. Yang, Y.X.; Ren, X.; Xu, Y. Main progress of adaptively robust filter with applications in navigation. *J. Navig. Position.* **2013**, *1*, 9–15.
21. Xu, Y.; Ahn, C.K.; Shmaliy, Y.S.; Chen, X.; Li, Y. Adaptive robust INS/UWB-integrated human tracking using UFIR filter bank. *Measurement* **2018**, *123*, 1–7. [[CrossRef](#)]
22. Fu, Z.; Han, Y. Centroid weighted Kalman filter for visual object tracking. *Measurement* **2012**, *45*, 650–655. [[CrossRef](#)]
23. Rigatos, G.; Siano, P.; Wira, P.; Busawon, K.; Binns, R. A nonlinear H-infinity control approach for autonomous truck and trailer systems. *Unmanned Syst.* **2020**, *8*, 49–69. [[CrossRef](#)]
24. Gustafsson, F. Particle filter theory and practice with positioning applications. *IEEE Aerosp. Electron. Syst. Mag.* **2010**, *25*, 53–82. [[CrossRef](#)]
25. Doucet, A.; Godsill, S.; Andrieu, C. On sequential Monte Carlo sampling methods for Bayesian filtering. *Stat. Comput.* **2000**, *10*, 197–208. [[CrossRef](#)]
26. Sun, W.; Liu, J.Z. Cooperative navigation method based on the Huber robust cubature fission particle filter. *Chin. J. Sci. Instrum.* **2022**, *43*, 166–175.
27. Aslan, M.F.; Durdu, A.; Sabanci, K.; Mutluer, M.A. CNN and HOG based comparison study for complete occlusion handling in human tracking. *Measurement* **2020**, *158*, 107704. [[CrossRef](#)]
28. Xia, X.; Hashemi, E.; Xiong, L.; Khajepour, A. Autonomous Vehicle Kinematics and Dynamics Synthesis for Sideslip Angle Estimation Based on Consensus Kalman Filter. *IEEE Trans. Control. Syst. Technol.* **2022**, *31*, 179–192. [[CrossRef](#)]
29. Liu, W.; Xia, X.; Xiong, L.; Lu, Y.; Gao, L.; Yu, Z. Automated Vehicle Sideslip Angle Estimation Considering Signal Measurement Characteristic. *IEEE Sens. J.* **2021**, *21*, 21675–21687. [[CrossRef](#)]
30. Xia, X.; Xiong, L.; Huang, Y.; Lu, Y.; Gao, L.; Xu, N.; Yu, Z. Estimation on IMU yaw misalignment by fusing information of automotive onboard sensors. *Mech. Syst. Signal Process.* **2021**, *162*, 107993. [[CrossRef](#)]
31. Gao, L.; Xiong, L.; Xia, X.; Lu, Y.; Yu, Z.; Khajepour, A. Improved Vehicle Localization Using On-Board Sensors and Vehicle Lateral Velocity. *IEEE Sens. J.* **2022**, *22*, 6818–6831. [[CrossRef](#)]
32. Zhang, F.X.; Yu, X.R.; He, W.F.; Li, C. Face recognition with improved loss function and multiple norm. *Comput. Eng. Appl.* **2020**, *56*, 144–150.
33. Izenman, A.J. *Modern Multivariate Statistical Techniques: Regression, Classification, and Manifold Learning*; Springer: New York, NY, USA, 2008.
34. Yang, Y.; He, H.; Xu, G. Adaptively robust filtering for kinematic geodetic positioning. *J. Geod.* **2001**, *75*, 109–116. [[CrossRef](#)]
35. Liu, W.; Xiong, L.; Xia, X.; Lu, Y.; Gao, L.; Song, S. Vision-aided intelligent vehicle sideslip angle estimation based on a dynamic model. *IET Intell. Transp. Syst.* **2020**, *14*, 1183–1189. [[CrossRef](#)]
36. Xia, X.; Meng, Z.; Han, X.; Li, H.; Tsukiji, T.; Xu, R.; Zhang, Z.; Ma, J. Automated Driving Systems Data Acquisition and Processing Platform. *arXiv* **2022**, arXiv:2211.13425.
37. Liu, W.; Quijano, K.; Crawford, M.M. YOLOv5-Tassel: Detecting tassels in RGB UAV imagery with improved YOLOv5 based on transfer learning. *IEEE J. Sel. Top. Appl. Earth Obs. Remote Sens.* **2022**, *15*, 8085–8094. [[CrossRef](#)]

Disclaimer/Publisher's Note: The statements, opinions and data contained in all publications are solely those of the individual author(s) and contributor(s) and not of MDPI and/or the editor(s). MDPI and/or the editor(s) disclaim responsibility for any injury to people or property resulting from any ideas, methods, instructions or products referred to in the content.